Smart Structures and Systems, *Vol. 27, No. 3 (2021) 525-536*
DOI: https://doi.org/10.12989/sss.2021.27.3.525

Analysis and optimization of a typical quasi-zero stiffness vibration isolator

Huan Li [1], Yang Yu [1], Jianchun Li*[1,2] and Yancheng Li**[1,3]

[1] *School of Civil and Environmental Engineering, Faculty of Engineering and Information Technology, University of Technology Sydney, Ultimo 2007, Australia*
[2] *Tianjin Key Laboratory of Civil Structure Protection and Reinforcement, Tianjin Chengjian University, Tianjin, 300384, China*
[3] *College of Civil Engineering, Nanjing Tech University, Nanjing 211800, China*

(*Received January 6, 2020, Revised October 28, 2020, Accepted January 15, 2021*)

Abstract. To isolate vibration at a low-frequency range and at the same time to provide sufficient loading support to the isolated structure impose a challenge in vibration isolation. Quasi-zero stiffness (QZS) vibration isolator, as a potential solution to the challenge, has been widely investigated due to its unique property of high-static & low-dynamic stiffness. This paper provides an in-depth analysis and potential optimization of a typical QZS vibration isolator to illustrate the complexity and importance of design optimization. By carefully examining the governing fundamentals of the QZS vibration isolator, a simplified approximation of force and stiffness relationship is derived to enable the characteristic analysis of the QZS vibration isolator. The explicit formulae of the amplitude-frequency response (AFR) and transmissibility of the QZS vibration isolator are obtained by employing the Harmonic Balance Method. The transmissibility curves under force excitation with different values of nonlinear coefficient, damping ratio, and amplitude of excitation are further investigated. As the result, an optimization of the structural parameter has been demonstrated using a comprehensive objective function with considering multiple dynamic characteristic parameters simultaneously. Finally, the genetic algorithm (GA) is adopted to minimise the objective function to obtain the optimal stiffness ratios under different conditions. General recommendations are provided and discussed in the end.

Keywords: quasi-zero stiffness; vibration isolation; dynamic characteristics optimization; genetic algorithm

1. Introduction

Vibration isolation technique is an effective vibration protection method for mechanical and civil structures. It has been widely used in numerous applications and becomes even more popular in recent years (Yu *et al*. 2020). The challenge in structural vibration isolation design is that to maintain load-carrying capacity requires sufficiently high stiffness while effective vibration isolation prefers the stiffness to be as lower as possible. This dilemma results in a difficult trade-off in a typical linear vibration isolator design. As the matter of fact, in the vibration isolation design, the isolation could only be effective when the designed stiffness is sufficiently low to ensure the frequency ratio of the excitation over natural frequencies is greater than $\sqrt{2}$. However, a very low system stiffness is not practical in maintaining structural stability and integrity. It will yield large deformation and cause the entire system to be unstable, especially under low and ultra-low frequency excitation (Carrella *et al*. 2008, Piersol and Harris 2017, Yu *et al*. 2019b). As a potential solution to this challenge, the idea of quasi-zero stiffness (QZS) vibration isolator has become popular and attracted a significant amount of attention in vibration isolation research. The promising potential that has been brought into the field is its characteristics of high-static & low-dynamic stiffness. The unique property endows the capacity to achieve effective vibration isolation while maintaining sufficient load-carrying capacity to the superstructure simultaneously.

The first attempt of the QZS vibration isolator can be traced back to the late Fifties when the original conceptual design was proposed by Molyneux (1958), of which the prototype is shown in Fig. 1. Based on this model, great efforts have been made by researchers and engineers in exploring novel designs and applications of the QZS vibration isolator. One of the main features in designing a QZS vibration isolator is to combine positive stiffness elements that are normally in form of mechanical springs and negative stiffness elements (Mizuno *et al*. 2007). There are four kinds of components commonly utilised as negative stiffness elements, including energy storage elements (e.g., springs and pre-buckled beams) (Winterflood *et al*. 2002, Le and Ahn 2011, Liu *et al*. 2013, Lan *et al*. 2014), magnetic elements (e.g., permanent magnets, electro-magnets, and hybrid magnets) (Carrella *et al*. 2008, Xu *et al*. 2013, Shi and Zhu 2015), geometrically nonlinear structures (e.g., cam and convex surface) (Zhou *et al*. 2015, Cheng *et al*. 2016), as well as composite structures and metamaterials (Chronopoulos *et al*. 2017). A comprehensive literature review on vibration isolators with negative stiffness property is described in detail by Li *et al*. (2020).

Over the past years, QZS vibration isolators have been extensively investigated to isolate vibration under low and

*Corresponding author, Professor,
E-mail: Jianchun.li@uts.edu.au
**Co-corresponding author, Ph.D.,
E-mail: Yancheng.li@uts.edu.au

ISSN: 1738-1584 (Print), 1738-1991 (Online)

ultra-low frequency range. Kashdan *et al*. (2012) and Fulcher *et al*. (2014) presented the results of the peak transmissibility about a meso-scale QZS system and verified that increasing the pre-compression of beam contributes to small peak transmissibility. Liu *et al*. (2013) and Huang *et al*. (2014) introduced buckled beams to a QZS vibration isolator and studied its force and displacement transmissibility. Niu *et al*. (2014) designed a novel QZS vibration isolator by employing a disk spring to replace the oblique springs in Fig. 1 and conducted parametric analysis on its stiffness, amplitude-frequency response (AFR), and transmissibility. Compared with a linear system, it could realize lower resonance frequency and smaller transmissibility. Zheng *et al*. (2016) investigated the effects of structural parameters on the stiffness and transmissibility of a QZS vibration isolator using magnetic springs. Zhou *et al*. (2015) and Cheng *et al*. (2016) presented a high-static & low-dynamic stiffness vibration isolator without direction limitation. The device could achieve two working states including contact state and detached state, which are suitable for both small and large amplitude excitations. Although QZS vibration isolators can reduce acceleration responses with low transmissibility, it sacrifices the displacement response, especially under large amplitude excitation (Viti *et al*. 2006, Lu and Lin 2009).

Combining QZS vibration isolator with damper to work as negative stiffness damper can provide a potential solution since damping device can dissipate vibration energy and reduce excessive displacement. Iemura and his co-workers proposed a negative stiffness damper that utilised the convex curve and sliding plate (Iemura *et al*. 2008, Iemura and Pradono 2009). The device could realize negative stiffness in the horizontal direction and was effective in mitigating structural acceleration response without amplifying displacement. Following that, Toyooka *et al*. (2015) presented a modified negative stiffness damper by introducing mechanical springs to provide pressure, which could work alone without requiring sufficient gravity. Sun *et al*. (2017) and Li *et al*. (2018) proposed a negative stiffness damper that integrated a negative stiffness device with a damper featuring a 20% damping ratio. It was applied to a highway bridge benchmark model, which realized a similar vibration isolation effect as a semi-active control device. Shi *et al*. (2018, 2019) proposed a re-centering negative stiffness damper which was verified to be able to reduce over 90% acceleration response without amplifying the deflection as the protection of damper. Bahar *et al*. (2018) combined a negative stiffness device with magneto-rheological dampers. The new integrated device could not only reduce the acceleration response but also the displacement response of the superstructures. Shi and Zhu (2019) conducted a comparative analysis to evaluate the pros and cons of negative stiffness damper and inerter damper with H2 and H∞ norms. The former is proved to be able to reduce both these two indices. However, as well known, overlarge damping in the vibration isolation system can suppress the vibration isolation effect, i.e., resulting in large transmissibility and large acceleration responses (Kelly 1999). That dilemma should be addressed in the design of a vibration isolator.

The design of a QZS vibration isolator is the task of obtaining desirable structural parameters to balance the contradictions between its properties which are important for maintaining its stability and functionality. To date, there has been very limited research on the optimization of QZS vibration isolators to guide the optimal selections of its structural parameters. By proposing the effective displacement range, Carrella *et al*. (2007a) conducted the static property optimization of a QZS vibration isolator. Comparing to its static properties, e.g., force and stiffness properties, its resonance frequency, AFR, and transmissibility as the dynamic characteristic parameters play more important roles in its vibration isolation performance. Moreover, these dynamic characteristic parameters influence each other in a complicated manner, which means it is inadequate to conduct trade-off on parameters separately. Hence, a comprehensive optimization of the structural parameters for the QZS vibration isolator by considering all these dynamic characteristics needs to be conducted.

This paper conducts an in-depth analysis of the properties and the potential optimization of the QZS vibration isolator. In particular, it focuses on a compact QZS vibration isolator proposed by Molyneux (1958). By applying the non-dimensional approach with using the supporting force of vertical spring as the cardinal number, the supporting force fluctuation rate and effective stiffness region are proposed to capture the fundamental behaviours of the QZS vibration isolator, which are adopted as the evaluation criteria to obtain the range of stiffness ratio. Besides, to investigate the dynamic characteristics of the QZS vibration isolator, approximate expressions of its non-dimensional force and stiffness are derived for simplifying calculation. The Harmonic Balance method is used to obtain the explicit formulae of its resonance frequency, AFR, and transmissibility in a similar way to Ravindra and Mallik (1994). In Section 4, the optimization requirements and the challenges, i.e., obtaining small resonance frequency, small AFR, and small transmissibility simultaneously, are raised and discussed. Following that, a comprehensive objective function for addressing these challenges is proposed to obtain the optimal stiffness ratio. Finally, the genetic algorithm (GA) is employed to minimise the objective function to attain the optimal stiffness ratios for different damping ratios and excitation amplitudes. Conclusions are given in Section 5 subsequently.

2. Fundamentals of QZS vibration isolator

The three-spring model is the simplest and most recognised QZS vibration isolator. In this design, the vertical spring provides positive stiffness and the two oblique springs contribute to negative stiffness. In Fig. 1, the system is at an undeformed position where the applied external force F will compress all three springs. When the two oblique springs move to the horizontal direction, the system is at its equilibrium position.

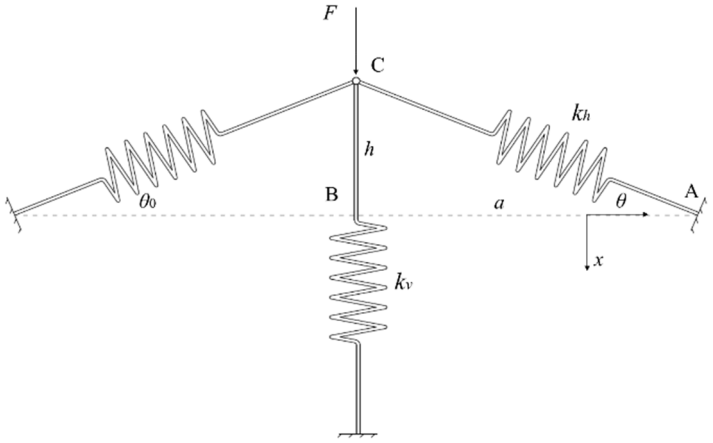

k_{h}	The stiffness of the oblique spring
k_{v}	The stiffness of the vertical spring
θ	The exact angle between oblique spring and horizontal direction
θ_0	The initial angle between the oblique spring and horizontal direction
a	The distance between point A and point B
h	The initial distance between point C and point B
$\lvert x \rvert$	The exact distance between point C and point B
L_0	The initial length of the oblique spring
L	The exact length of the oblique spring

Fig. 1 The three-spring model

2.1 Non-dimensional force

For a vibration isolator, sufficient static load-carrying capacity is an essential requirement for supporting the weight of the isolated structure. When the external force drives the system to move from its initial position C to its equilibrium position B, a vertical reactive force will be generated to balance the external force. The reactive force is the resultant of vertical spring force and the vertical components of the two oblique spring forces, which is described by Eq. (1). (Note: the origin of coordinates is set at point B)

$$F_{\mathrm{total-v}} = F_{\mathrm{v}} + 2F_{\mathrm{h-v}} \tag{1}$$

Vertical forces from the vertical spring and two oblique springs are derived as follows where the minus sign represents the negative direction of the coordinate

$$F_{\mathrm{v}} = -k_{\mathrm{v}}(h - x) \tag{2}$$

$$F_{\mathrm{h-v}} = -k_{\mathrm{h}}(L_0 - L)\sin\theta \tag{3}$$

$$L_0 = \sqrt{a^2 + h^2},\ L = \sqrt{a^2 + x^2} = x/\sin\theta \tag{4}$$

Substituting Eqs. (2)-(4) into Eq. (1) and obtaining

$$\begin{aligned} F_{\mathrm{total-v}} &= F_{\mathrm{v}} + 2F_{\mathrm{h-v}} \\ &= -k_{\mathrm{v}}h + (k_{\mathrm{v}} + 2k_{\mathrm{h}})x \\ &\quad -2k_{\mathrm{h}}\sqrt{a^2 + h^2}\frac{x}{\sqrt{a^2 + x^2}} \end{aligned} \tag{5}$$

Here, we define the following parameters

$$\begin{aligned} &\text{Non-dimensional force:} \quad \hat{F} = \frac{F_{\mathrm{total-v}}}{k_{\mathrm{v}}h}, \\ &\text{Stiffness ratio:} \quad \alpha = \frac{k_{\mathrm{h}}}{k_{\mathrm{v}}}, \\ &\text{Initial incline ratio:} \quad \beta_0 = \frac{a}{h} = \cot\theta_0, \\ &\text{Non-dimensional displacement:} \quad \hat{x} = \frac{x}{h} \end{aligned} \tag{6}$$

In the published research, $k_{\mathrm{v}}L_0$ is commonly used as the cardinal number to conduct the non-dimensional process. It is a composite parameter including the stiffness of vertical spring and the length of the oblique spring (Carrella *et al*. 2007b, Le and Ahn 2011). Although this parameter can be used to simplify the equation, there is no clear physical meaning, which results in that the obtained non-dimensional force cannot reflect the change of load-carrying capacity of the QZS vibration isolator. To simplify the force and assign non-dimensional force with physical meaning, $k_{\mathrm{v}}h$ is defined as the cardinal number. It is the restored elastic force of the vertical spring when the device is at the equilibrium position. A larger value of $k_{\mathrm{v}}h$ indicates a higher load-carrying capacity. Hence, the value of non-dimensional force can be used to represent the fluctuation of the supporting force of the QZS vibration isolator and the relative position of point C during motion. Besides, a new parameter, the initial incline ratio β_0, is defined to reflect the initial position of these three springs.

Substituting Eq. (6) into Eq. (5), the non-dimensional force of the QZS vibration isolator is derived as Eq. (7) that is composed of a constant, a linear term, and a nonlinear term.

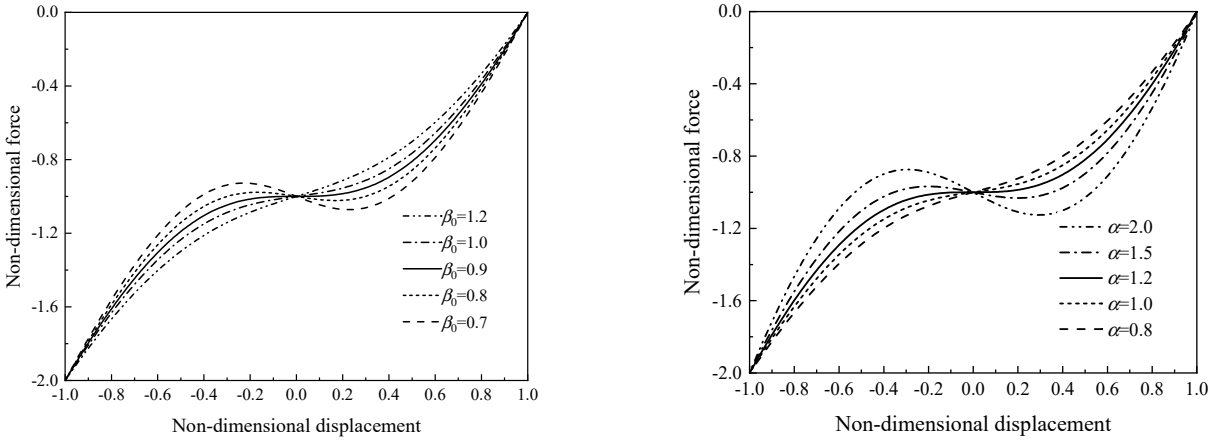

(a) Under different values of β_0 (b) Under different values of α

Fig. 2 The relationship between non-dimensional force and non-dimensional displacement

$$\hat{F} = \frac{F_{\text{total-v}}}{k_{\text{v}}h} = -1 + (1+2\alpha)\hat{x} - 2\alpha\sqrt{\beta_0^2+1}\frac{\hat{x}}{\sqrt{\beta_0^2+\hat{x}^2}} \tag{7}$$

In addition to non-dimensional displacement, stiffness ratio α and initial incline ratio β_0 also determine the values of non-dimensional force. The relationships between non-dimensional force and non-dimensional displacement under different α and β_0 are shown in Fig. 2. All these curves are symmetric about the equilibrium point B, where the non-dimensional force is -1. The nonlinear degree of the non-dimensional force is enhanced with β_0 decreasing and α increasing. The slopes of these curves can be positive, zero, and negative around the equilibrium position and the QZS vibration isolator can achieve a typical negative stiffness bistable curve.

2.2 Non-dimensional stiffness

By differentiating Eq. (7) with respect to non-dimensional displacement, the non-dimensional dynamic stiffness of the QZS vibration isolator is described as

$$\hat{K} = 1 + 2\alpha\left[1 - \frac{\beta_0^2\sqrt{\beta_0^2+1}}{(\beta_0^2+\hat{x}^2)^{\frac{3}{2}}}\right] \tag{8}$$

The relationship between non-dimensional stiffness and non-dimensional displacement is plotted in Fig. 3. When the two oblique springs are in the horizontal equilibrium position, the stiffness is minimum which can be positive, zero, and negative stiffness. Negative stiffness is unstable in nature and it does not have load-carrying capacity. Excessive stiffness leads to ineffective vibration isolation. Hence, if the total stiffness of the isolator is set to be zero or small positive stiffness at its equilibrium position, it will keep stable and realize desirable vibration isolation effect simultaneously. By letting Eq. (8) equal to zero at the equilibrium position, the relationship between β_0 and α are obtained as

$$\beta_0 = \sqrt{\frac{4\alpha^2}{(4\alpha+1)}} \tag{9}$$

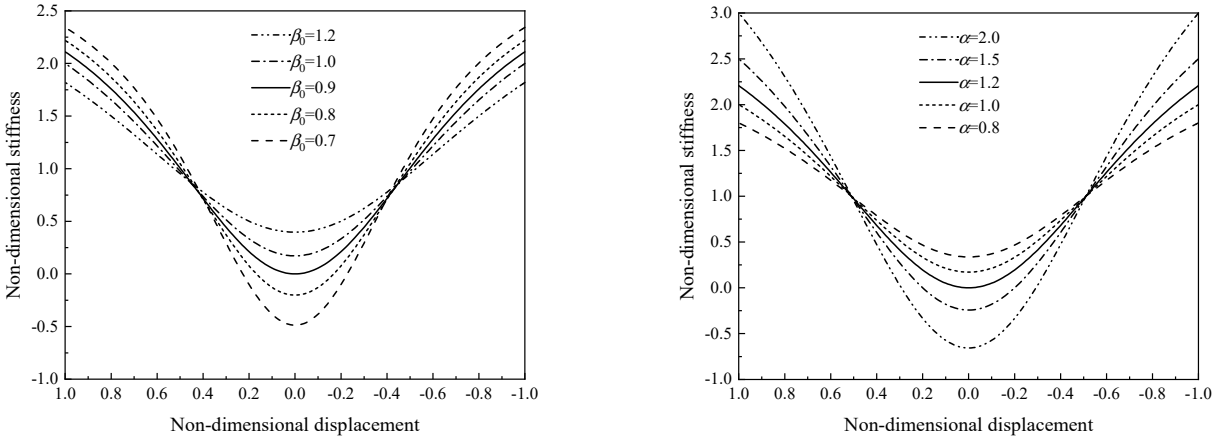

(a) Under different values of β_0 (b) Under different values of α

Fig. 3 The relationship between non-dimensional stiffness and non-dimensional displacement

Then Eq. (7) and Eq. (8) can be subsequently expressed as

$$\hat{F} = -1 + (1 + 2\alpha)\hat{x} - \frac{2\alpha(1 + 2\alpha)\hat{x}}{\sqrt{4\alpha^2 + \hat{x}^2(4\alpha + 1)}} \tag{10a}$$

$$\hat{K} = 1 + 2\alpha[1 - \frac{4\alpha^2(1 + 2\alpha)}{(4\alpha^2 + \hat{x}^2(4\alpha + 1))^{\frac{3}{2}}}] \tag{10b}$$

2.3 Supporting force fluctuation rate and effective stiffness region

Based on Eqs. (10a) and (10b), in Fig. 4, the QZS vibration isolator designed with different stiffness ratios presents various performances. The values of non-dimensional force and non-dimensional stiffness change significantly with point C moving away from the equilibrium position. It is advantageous if a QZS vibration isolator can maintain sufficient load-carrying capacity and low dynamic stiffness during a wide working displacement region around the equilibrium position.

In Fig. 4, two parameters including supporting force fluctuation rate and effective stiffness region are defined to evaluate the static performance of the QZS vibration isolator. In Fig. 4(a), when point C moves to a specific point (for instance, $\hat{x} = -0.5$), the supporting force fluctuation rate is the ratio of the non-dimensional force variation relative to that at equilibrium position over -1 (the value of non-dimensional force at the equilibrium position), which is described by Eq. (11). In Fig. 4(a), when α is equal to 0.1, 0.5, and 1.0, the supporting force fluctuation rates are about 41%, 24%, and 19%, respectively. According to Fig. 5(a), a small stiffness ratio results in a large supporting force fluctuation rate especially when the stiffness ratio is smaller than 0.35, which is undesirable for maintaining stable load-carrying capacity. Besides, over 90% reduction of the supporting force fluctuation rate happens when α is smaller than 2.0.

$$R = \left|(1 + 2\alpha)\hat{x} - \frac{2\alpha(1 + 2\alpha)\hat{x}}{\sqrt{4\alpha^2 + \hat{x}^2(4\alpha + 1)}}\right| \times 100\% \tag{11}$$

$$E = 2\sqrt{\frac{4\alpha^2((\frac{1+2\alpha}{2\alpha - K_{\lim}+1})^{\frac{2}{3}} - 1)}{(4\alpha + 1)}} \tag{12}$$

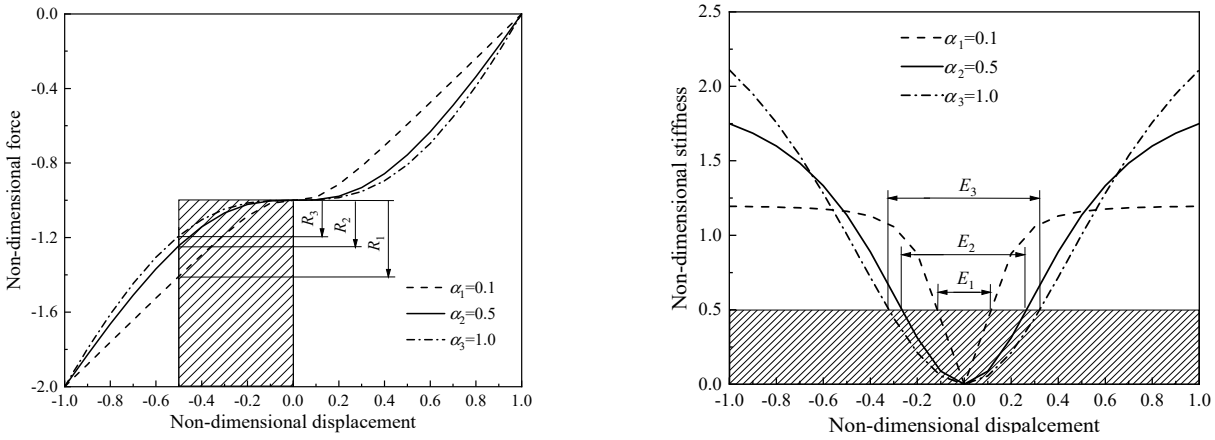

(a) Non-dimensional force (b) Non-dimensional stiffness

Fig. 4 The static properties of the QZS vibration isolator

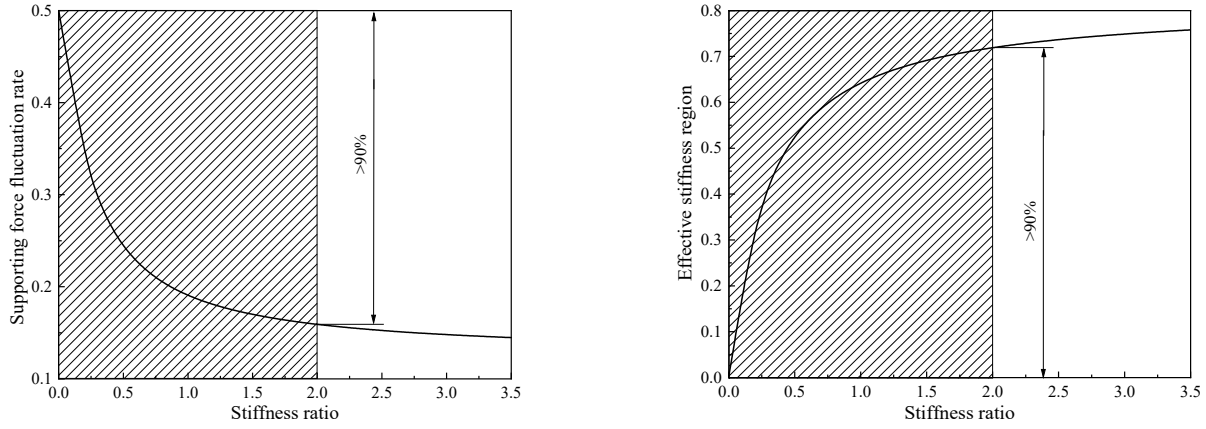

(a) Supporting force fluctuation rate (b) Effective stiffness region

Fig. 5 The effects of stiffness ratio on static properties of the QZS vibration isolator

The effective stiffness region is the displacement region under where the non-dimensional stiffness is smaller than a threshold value K_{lim}. It can be derived by letting Eq. (10a) to be smaller than K_{lim} and the solution is expressed by Eq. (12). When $K_{\text{lim}} = 1$, the non-dimensional stiffness is equal to that of vertical spring alone, which means the oblique springs provide zero stiffness. In Fig. 4(b), the effective stiffness regions for $K_{\text{lim}} = 0.5$ are 0.22, 0.53, and 0.64 for the cases that α equals to 0.1, 0.5, and 1.0, respectively. Similarly, Fig. 5(b) indicates that a large stiffness ratio is effective for attaining a large effective stiffness region, while the effect will be insignificant when α is larger than 2.0. Besides, although a large stiffness ratio is desirable for obtaining both a small supporting force fluctuation rate and large effective stiffness region, it requires very strong oblique springs especially for the cases that need high load-carrying capacity, which is undesirable and uneconomic. Hence, the optimal ranges of β_0 and α are set to 0.45~1.33 and 0.35~2.00, respectively.

2.4 Approximate and simplified force and stiffness

Due to the complex relationships between the non-dimensional force and displacement, as well as non-dimensional stiffness and displacement, it is not convenient to conduct further calculations to analyse the dynamic characteristics of the QZS vibration isolator. Since the curves in Fig. 4(a) present an almost cubic relationship between the non-dimensional force and displacement, Taylor series expansion is adopted to simplify the relationship to a power series of order 3 in Eq. (13). Similarly, by enforcing the condition on α and β_0 in Eq. (9) to make the non-dimensional stiffness zero at the equilibrium position, Eq. (13) is simplified as Eq. (14).

$$\hat{F}^* = -1 + \left(1 + 2\alpha - 2\alpha\frac{\sqrt{\beta_0^2+1}}{\beta_0}\right)\hat{x} + \alpha\frac{\sqrt{\beta_0^2+1}}{\beta_0^3}\hat{x}^3 \tag{13}$$

$$\hat{F}^* = -1 + \frac{(2\alpha+1)(4\alpha+1)}{8\alpha^2}\hat{x}^3 \tag{14}$$

Differentiating $\hat{F}^*$ with respect to $\hat{x}$, the simplified non-dimensional stiffness is described as

$$\hat{K}^* = \frac{3(2\alpha+1)(4\alpha+1)}{8\alpha^2}\hat{x}^2 \tag{15}$$

3. Dynamic characteristics of QZS vibration isolation system

3.1 Amplitude-frequency response

A single-degree-of-freedom spring-mass-damping system is used to illustrate the functionality of a QZS vibration isolation system. In Fig. 6, a cosine force is applied to the mass, which usually presents the disturbance

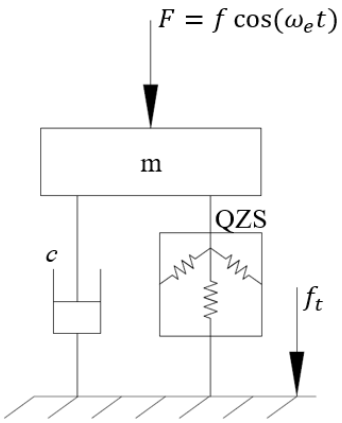

Fig. 6 Schematic of a one-degree-of-freedom nonlinear vibration isolation system

from equipment or machine. For this QZS vibration isolation system, its equation of motion under the excitation force F is expressed by the following equation.

$$m\ddot{x} + c\dot{x} + F(x) - mg = F \tag{16}$$

where $mg = -k_v h$, $F = f\cos(\omega_e t)$, and $F(x)$ is the nonlinear force provided by the QZS vibration isolator.

Eq. (16) can be simplified as follows.

$$\ddot{\hat{x}} + 2\xi\dot{\hat{x}} + \frac{(2\alpha+1)(4\alpha+1)}{8\alpha^2}\hat{x}^3 = \hat{f}\cos(\gamma\tau) \tag{17}$$

where $\tau = \omega_n t$, $\gamma = \frac{\omega_e}{\omega_n}$, $\omega_n = \sqrt{\frac{k_v}{m}}$, $\xi = \frac{c}{2m\omega_n}$, $\hat{x} = \frac{x}{h}$, and $\hat{f} = \frac{f}{k_v h}$. Note that ω_n is the natural frequency of the system around the equilibrium position, which can be regarded as a constant when the vibration amplitude is small. By introducing nonlinear coefficient $\mu = \frac{(2\alpha+1)(4\alpha+1)}{8\alpha^2}$ that is negatively correlated with stiffness ratio, the uniform differential equation of motion for this system and other equivalent QZS vibration isolation systems can be given by Eq. (18).

$$\ddot{\hat{x}} + 2\xi\dot{\hat{x}} + \mu\hat{x}^3 = \hat{f}\cos(\gamma\tau) \tag{18}$$

This is the Duffing equation of the nonlinear system under force excitation. The Harmonic Balance Method is used to obtain the analytic solution of it (Brennan *et al*. 2008, Zheng *et al*. 2018). The AFR is obtained and given by Eq. (19). Its two positive solutions are obtained as follows.

$$(\frac{3}{4}\mu A^3 - \gamma^2 A)^2 + 4\xi^2\gamma^2 A^2 = \gamma^4 \tag{19}$$

$$\gamma_{1,2} = 0.5\sqrt{3\mu A^2 - 8\xi^2 \pm \frac{4}{A}\sqrt{4\xi^4 A^2 - 3\mu\xi^2 A^4 + f^2}} \tag{20}$$

The maximum AFR ($A_{\max}$), as well as the corresponding resonance frequency of this nonlinear system described by Eqs. (21) and (22), can be obtained by

equating the two results in Eq. (20). If $\xi^6 \ll \frac{3}{4}\mu\hat{f}^2$, the resonance frequency can be simplified as Eq. (23). A desirable vibration isolation system should be able to isolate vibration during a wide frequency range, which requires low resonance frequency. The $A_{\max}$ is influenced by nonlinear coefficient (related to stiffness ratio), damping ratio and amplitude of excitation. In practice, the devices are always connected with other elements or there is always space limitation, which requires $A_{\max}$ to be within a threshold value to avoid large deflection.

$$A_{\max} = \sqrt{\frac{2\xi^3 + \sqrt{4\xi^6 + 3\mu f^2}}{3\mu\xi}} \tag{21}$$

$$\gamma_{\text{res}} = \frac{1}{\sqrt{2\xi}} \sqrt{\sqrt{\xi^6 + \frac{3}{4}\mu\hat{f}^2} - 3\xi^3} \tag{22}$$

$$\gamma_{\text{res}} \approx \sqrt[4]{\frac{3\mu\hat{f}^2}{16\xi^2}} \tag{23}$$

The AFR curve is shown in Fig. 7. Compared with the linear system, the AFR curve of this QZS vibration isolation system bends to the right, which is a hardening system. When the frequency ratio γ is small, the effect of the QZS vibration isolation system is less effective than that of the equivalent linear system. However, with γ increasing, its advantages gradually appear, e.g., small γ_{res} and small AFR. Besides, in a linear system, there is always one certain amplitude response for each γ and a peak value arises when γ equals to 1. Compared with that, there are several steady-state response solutions between γ_{res} and γ_{up} for the QZS vibration isolation system. When the excitation frequency increases, the amplitude jumps down suddenly from points J_1 to J_3 instead of changing along the curve from J_1 to J_3. Vice versa, it will jump up from J_2 to J_4. Therefore, the QZS vibration isolation system is unstable between the jump-down frequency γ_{res} and jump-up frequency γ_{up}. Due to the fact that drop-jump phenomenon results in undesirable and destructive effects between γ_{up} and γ_{res}, it is important to ensure that there is a unique amplitude response at each frequency ratio. By equalizing γ_{res} and γ_{up}, the jump avoidance condition is obtained (Malatkar and Nayfeh 2002, Brennan *et al*. 2008). As long as the damping ratio is larger than the threshold-damping ratio ξ_{th}, the drop-jump phenomenon can be avoided. According to Eq. (24), the threshold-damping ratio is decided by the amplitude of excitation force and nonlinear coefficient.

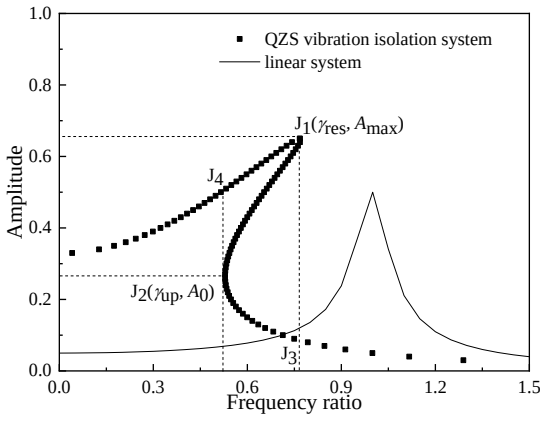

Fig. 7 The AFR curves ($\alpha = 1, \mu = 1.875, \xi = 0.05, \hat{f} = 0.05$)

$$\xi_{\text{th}} \approx \left(\frac{\hat{f}}{36}\right)^{1/3} \left(\frac{\mu}{3}\right)^{1/6} \tag{24}$$

3.2 Transmissibility

Compared with a linear vibration isolator, one of the main advantages of a QZS vibration isolator is that it can attain small transmissibility with low dynamic stiffness without sacrificing the load-carrying capacity. Force transmissibility is defined as the ratio of the transmitted force and the excitation force. In Eq. (25), the force transmitted from the vibration source to the base through the nonlinear system is composed of two parts, i.e., non-dimensional elastic force transmitted through the springs and non-dimensional damping force transmitted through the damper, which are given by Eq. (26).

$$\hat{f}_T = \hat{f}_s + \hat{f}_d = \mu\hat{x}^3 + 2\xi\dot{\hat{x}} \tag{25}$$

$$\hat{f}_{\text{T}} = \frac{3}{4}\mu A^3 \cos(\gamma\tau + \varphi) - 2\xi\gamma A\sin(\gamma\tau + \varphi) \tag{26}$$

Because the phase difference of non-dimensional elastic force and non-dimensional damping force is $\frac{\pi}{2}$, the non-dimensional force transmitted to the base can be calculated as follows.

$$\begin{aligned}\hat{f}_{\text{T}} &= \sqrt{\left(\frac{3}{4}\mu A^3\cos(\gamma\tau + \varphi)\right)^2 - \left(2\xi\gamma A\sin(\gamma\tau + \varphi)\right)^2} \\ &= \sqrt{\frac{9}{16}\mu^2 A^6 + 4\xi^2\gamma^2 A^2}\end{aligned} \tag{27}$$

Then the force transmissibility of this system is expressed as Eq. (28), which is determined by frequency ratio, damping ratio, nonlinear coefficient, and the amplitude of excitation force.

$$T = \frac{\hat{f}_{\text{T}}}{\hat{f}} = \sqrt{\frac{\frac{9}{16}\mu^2 A^6 + 4\xi^2\gamma^2 A^2}{f^2}} \tag{28}$$

By substituting Eqs. (21) and (23) to Eq. (28), the peak force transmissibility is obtained as follows.

$$T_{\max} = \sqrt{\frac{\frac{9}{16}\mu^2 {A_{\max}}^6 + 4\xi^2 {\gamma_{\text{res}}}^2 {A_{\max}}^2}{\hat{f}^2}} \tag{29}$$

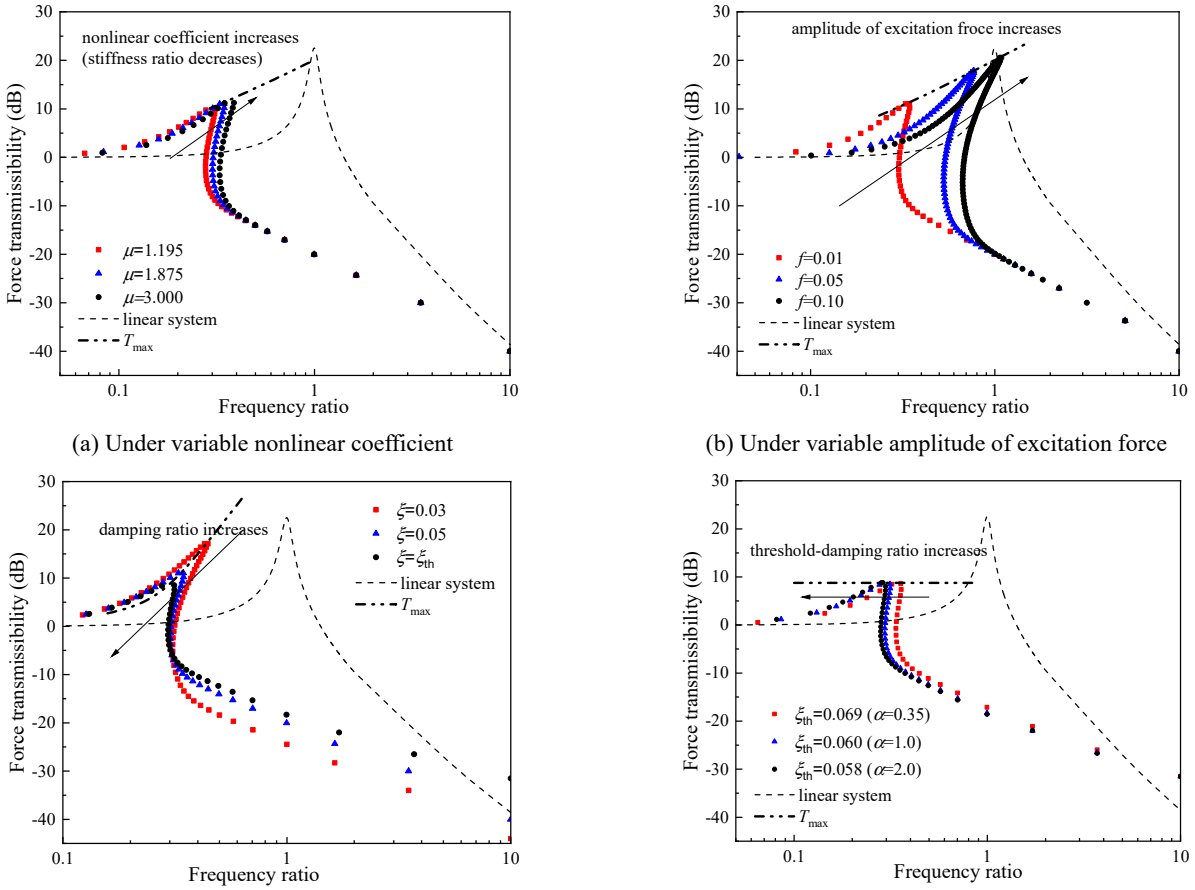

(a) Under variable nonlinear coefficient

(b) Under variable amplitude of excitation force

(c) Under variable damping ratio

(d) Under threshold-damping ratio

Fig. 8 The relationship between force transmissibility and frequency ratio

$$T_{\text{linear}} = \sqrt{\frac{1+(2\xi\gamma)^2}{(1-\gamma^2)^2+(2\xi\gamma)^2}} \tag{30}$$

The force transmissibility of a linear system is derived as Eq. (30), which is only related to damping ratio and frequency ratio.

The effects of nonlinear coefficient, amplitude of excitation, damping ratio, and threshold-damping ratio on force transmissibility under different frequency ratios are shown in Fig. 8. The transmissibility is expressed by dB that is calculated by $20\log_{10}T$. The transmissibility of the corresponding linear system is depicted by the dashed line. It reaches its maximum value and resonance happens when the frequency ratio is equal to 1. Similar to AFR, the transmissibility curves of the QZS vibration isolation system also bend to the right and its advantages over the linear system become significant with frequency ratio increasing, e.g., small transmissibility and low γ_{res}.

In Fig. 8(a), around the resonance frequency region, with the nonlinear coefficient decreasing, the peak force transmissibility $T_{\max}$ and resonance frequency γ_{res} are attenuated. The nonlinear coefficient has no effect on the transmissibility when the frequency ratio is larger than the resonance frequency. According to Fig. 8(b), under moderate excitation with a small amplitude, the γ_{res} and $T_{\max}$ of the QZS vibration isolation system are much smaller than that of the linear system. However, the increase of excitation amplitude gradually weakens these advantages, because the stiffness of the QZS vibration isolator increases significantly outside the effective stiffness region. In Figs. 8(c) and (d), a large damping ratio enables the system to suppress resonance response and realize low resonance frequency. Moreover, a larger damping ratio is also desirable for narrowing the unstable drop-jump region. The unstable region will disappear and $T_{\max}$ will be a constant, if damping ratio is set to the threshold-damping ratio. However, large damping ratio leads to large transmissibility and acceleration responses during the vibration isolation region. Hence, there is a trade-off in selecting a reasonable damping ratio during the design of a QZS vibration isolator.

4. Dynamic characteristics optimization of QZS vibration isolator

A favourable vibration isolator is expected to minimise the transmission of vibration during a wide frequency range, i.e., realizing low transmissibility and low resonance frequency. In the meantime, it should be able to maintain the stability of the entire system by effectively controlling the displacement response of the system, e.g., avoiding excessive deformation and deformation fluctuation,

especially for the situation with space limitation. To satisfy the requirements, a comprehensive optimization is proposed to obtain the optimal stiffness ratio for the QZS vibration isolator.

4.1 Optimization requirements and objective function

As discussed in Section 2 and Section 3, the supporting force fluctuation rate and effective stiffness region are decided by the stiffness ratio, based on which the optimal range of stiffness ratio is obtained as 0.35~2.00. The effects of the stiffness ratio (nonlinear coefficient), damping ratio, and amplitude of excitation on the dynamic characteristics of the QZS vibration isolation system, i.e., resonance frequency, AFR, and transmissibility are analysed and plotted in Fig. 9. Here, the normalised non-dimensional magnitude ($Y_i = \frac{(y)_i}{(y)_{\max}}$) of each dynamic characteristic parameter that varies from 0 to 1 is calculated.

Fig. 9(a) shows that $T_{\max}$ and γ_{res} decrease with stiffness ratio increasing, while $A_{\max}$ increases during this process. The effects of stiffness ratio on γ_{res}, $A_{\max}$ and $T_{\max}$ are contradictory, which requires a comprehensive optimization to determine a favourable stiffness ratio based on the working conditions and practical requirements. In Fig. 9(b), a large damping ratio is desirable for obtaining small γ_{res}, $A_{\max}$ and $T_{\max}$. Besides, when the damping ratio is larger than the threshold-damping ratio, the effects become insignificant. By considering the undesirable effect of large damping ratio in the vibration isolation region and the avoidance condition of the drop-jump phenomenon, the damping ratio can be set to or slightly greater than the threshold-damping ratio. To investigate the influence of damping ratio on the optimization results, the scenarios with different damping ratios will be investigated, including ξ= 0.05 and ξ= threshold-damping ratio. As shown in Fig. 9(c), all these three dynamic characteristic parameters are amplified with the increase of the excitation amplitude f, which can raise the vibration responses of the QZS vibration isolator. Besides, the amplitude of excitation varies constantly in practice, which is uncontrollable and unpredictable. Hence, it is taken as a conditional parameter instead of an optimal parameter and the scenarios with different excitation amplitudes will be analysed.

Based on the analysis of the dynamic characteristic parameters of the QZS vibration isolator, several optimization requirements are proposed, which are described by Eqs. (31)-(33). Although, the jump phenomenon reflects the stability of the system, it is not defined as one of the optimization requirements since it can be avoided when the damping ratio is larger than the threshold-damping ratio ξ_{th}.

(a) Small γ_{res} makes the system be able to work under a wide working frequency region without resonance;

$$\text{minimise}\,(\gamma_{\text{res}}) \rightarrow \text{minimise}\left(\frac{3\mu\hat{f}^2}{16\xi^2}\right)^{\frac{1}{4}} \tag{31}$$

(b) Small $A_{\max}$ represents the high stability and effective vibration suppression of the system;

$$\text{minimise}\,(A_{\max}) \rightarrow \text{minimise}\left(\sqrt{\frac{2\xi^3+\sqrt{4\xi^6+3\mu f^2}}{3\mu\xi}}\right) \tag{32}$$

(c) Small $T_{\max}$ reflects the desirable vibration isolation performance of the system;

$$\text{minimise}\,(T_{\max}) \rightarrow \text{minimise}\left(\sqrt{\frac{\frac{9}{16}\mu^2A^6+4\xi^2\gamma^2A^2}{f^2}}\right) \tag{33}$$

Based on these optimization requirements, a comprehensive objective function for obtaining the optimal stiffness ratio (or nonlinear coefficient) is proposed. As described by Eq. (34), three normalised non-dimensional magnitude factors are included, and in the meantime, three weighting coefficients are defined to represent the

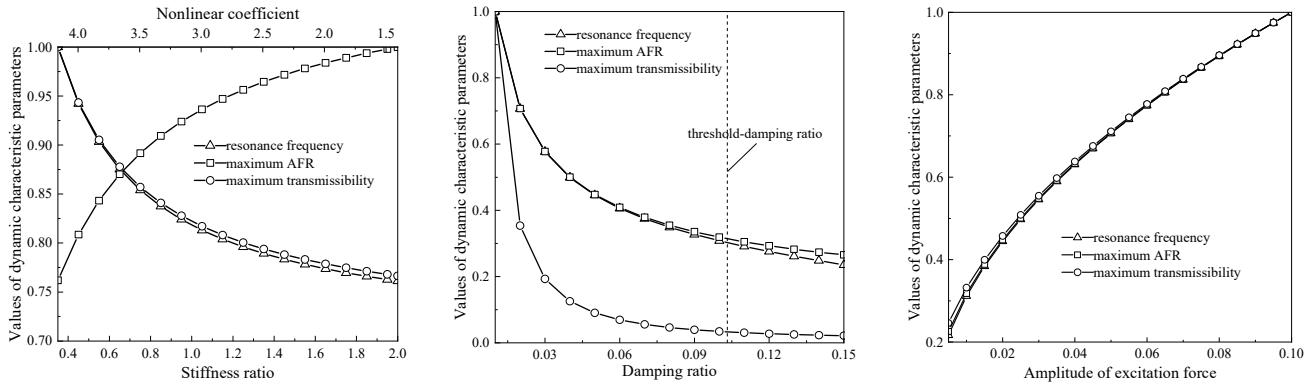

(a) Under stiffness ratio (b) Under damping ratio (c) Under amplitude of excitation force

Fig. 9 The effects of system parameters on the values of dynamic characteristic parameters Note: the normalised non-dimensional magnitude of each dynamic characteristic parameter=the values of each dynamic characteristic parameter/its maximum values during the range

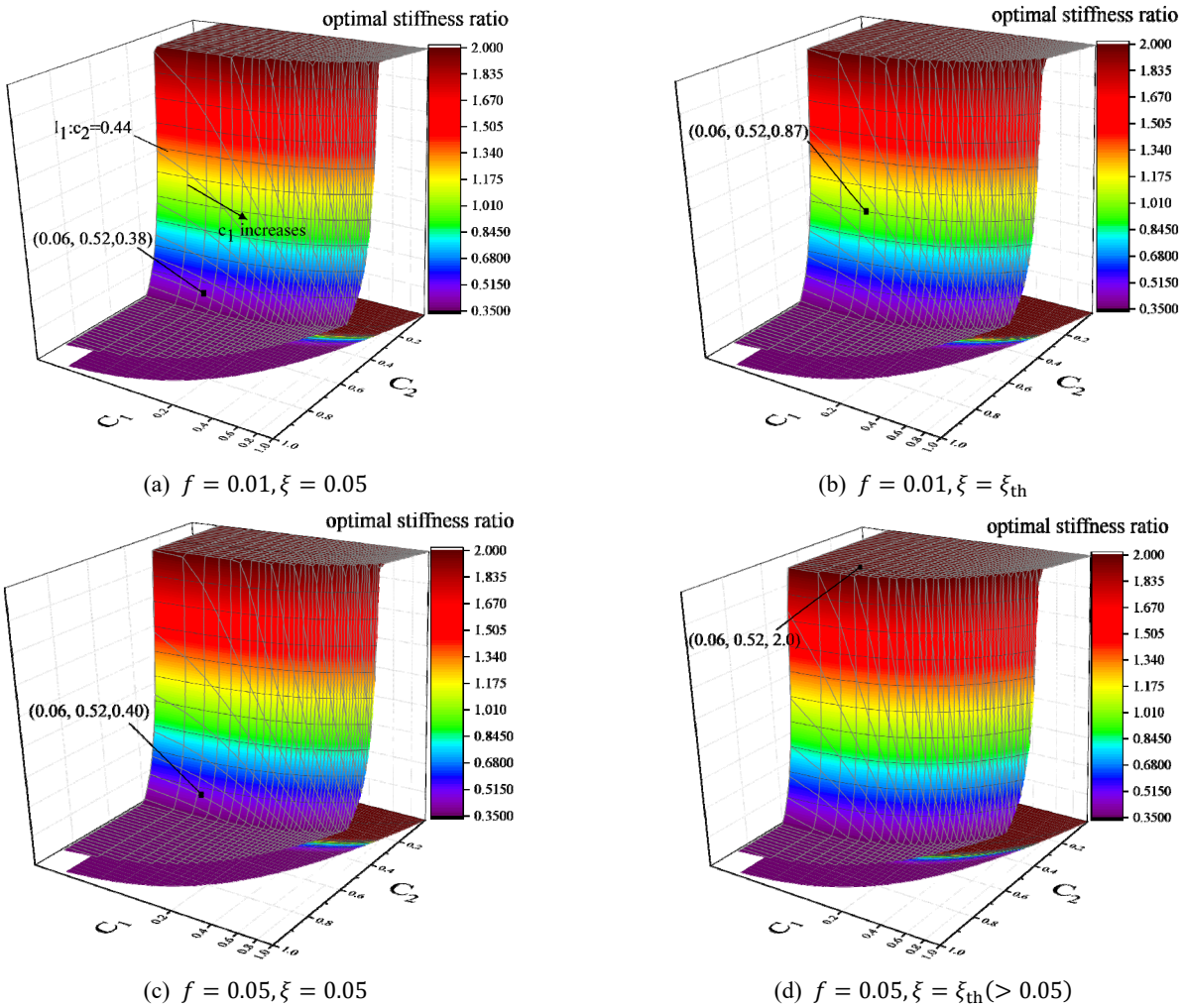

(a) $f = 0.01, \xi = 0.05$ (b) $f = 0.01, \xi = \xi_{\text{th}}$

(c) $f = 0.05, \xi = 0.05$ (d) $f = 0.05, \xi = \xi_{\text{th}} (> 0.05)$

Fig. 10 The optimization results with different values of damping under different amplitudes of excitation

importance of each factor. The designers can set these three weighting coefficients to different values based on the working conditions and practical requirements of the QZS vibration isolation system. The optimization problem aims to attain the optimal stiffness ratio to minimise Eq. (34) under different damping ratios and excitation amplitudes.

$$O_i = c_1 \frac{(\gamma_{\text{res}})_i}{(\gamma_{\text{res}})_{\max}} + c_2 \frac{(A_{\max})_i}{(A_{\max})_{\max}} + c_3 \frac{(T_{\max})_i}{(T_{\max})_{\max}} \quad (34)$$

where $c_1 + c_2 + c_3 = 1$ and $0 \le c_1, c_2, c_3 \le 1$.

4.2 Optimization method and results

In this study, the GA, with the benefits of easy coding and fast convergence (Yu *et al.* 2019a), is selected to solve the optimization problem. The implementation of GA is based on the Matlab 2015a Optimization toolbox. The algorithm parameter setting of GA is given as follows: the chromosome number N = 20, the maximum iteration number T = 100, the crossover probability p_c = 0.7, and the mutation probability p_m = 0.01. The range of the parameter (stiffness ratio) to be identified is from 0.35 to 2.00. In the optimization evolution, the roulette wheel strategy is adopted to select part of the chromosome to generate a new chromosome. In the GA, the algorithm will be terminated when the maximum iteration number is reached. Then, the objective function (Eq. (34)) with different weighting coefficients is solved by the GA for the optimal solution, the results of which will be presented and analysed in the following part.

The influences of the weighting coefficients c_1 and c_2 (c_3 is determined by c_1 and c_2) on the optimal stiffness ratio α are shown in Fig. 10. These four 3D surfaces demonstrate that when c_2 close to 0, α is equal to its maximum. With c_2 increasing, the optimal stiffness ratio decreases significantly, which equals to 0.35 when c_2 approaches to 1. That is because when the most important coefficient is c_2, the weight of $A_{\max}$ in Eq. (34) is the largest, hence requiring a small stiffness ratio. c_1 also has profound effect on the optimal stiffness ratio. According to the line 1 with a constant c_2 in Fig. 10(a), the increasing of c_1 bends the line to small optimal stiffness ratio. The marked points in Fig. 10 illustrate that when $c_1 = 0.06$, $c_2 = 0.52$, and $c_3 = 0.42$, the optimal stiffness ratio are 0.38, 0.87, 0.40 and 2.0 respectively for these four scenarios.

Based on Figs. 10(a) and (c), large excitation amplitude f contributes to a slight increase of optimal α. Hence,

relatively strong oblique springs are required for designing the QZS vibration isolator working under strong excitation. By comparing Figs. 10(a) with (b) and Figs. 10(c) with (d), it shows that a large damping ratio can lead to the increase of the optimal stiffness ratio and the area of $\alpha = 2$. That is because the increase of damping ratio contributes to the reduction of $A_{\max}$ (Fig. 9(b)), which weakens its influence in the objective function. Therefore, strong oblique springs are desirable for the scenario with a large damping ratio and strong excitation. For the working condition with displacement limitation, the oblique springs should be relatively soft.

5. Conclusions

In this paper, an in-depth investigation of the characteristics of a compact three-spring QZS vibration isolator is conducted, which is the original model for a series of existing devices. Hence, the research methods and results can be generally applied to analyse other modified QZS vibration isolators. An alternative formulation for the force and stiffness with $k_v L_0$ as the cardinal number is presented to better reflect the physical meaning and capture the fundamentals of the QZS vibration isolator. Following that, the supporting force fluctuation rate and effective stiffness region are defined to evaluate its static properties, based on which the recommended ranges for the stiffness ratio α and the initial incline ratio β_0 are set to 0.35~2.00 and 0.45~1.33, respectively.

To address the contradiction between obtaining low resonance frequency, small maximum transmissibility, and small maximum AFR, a comprehensive optimization is conducted in this paper to attain the optimal stiffness ratio. The proposed unique optimization objective function considers all these three characteristic parameters with setting different weight coefficients. Generally, during the optimization process, three weight coefficients should be determined first according to the working conditions. Then based on the excitation amplitude and damping ratio, the optimal stiffness ratio can be obtained by minimising the objective function utilising GA. The optimal results demonstrate that stronger oblique springs are desirable for the working conditions with larger excitation amplitude and (or) damping ratio. However, the optimal stiffness ratio should be limited to a relatively small value when there are deformation constraints.

Acknowledgments

The authors would like to acknowledge the research funding from Australian Research Council under Discovery Project Scheme (DP150102636) to support PhD scholarship in conducting this research.

References

Bahar, A., Salavati-Khoshghalb, M. and Ejabati, S.M. (2018), "Seismic protection of smart base-isolated structures using negative stiffness device and regulated damping", *Smart Struct. Syst., Int. J.*, **21**(3), 359-371. https://doi.org/10.12989/sss.2018.21.3.359

Brennan, M., Kovacic, I., Carrella, A. and Waters, T. (2008), "On the jump-up and jump-down frequencies of the Duffing oscillator", *J. Sound Vib.*, **318**(4-5), 1250-1261. https://doi.org/10.1016/j.jsv.2008.04.032

Carrella, A., Brennan, M. and Waters, T. (2007a), "Optimization of a quasi-zero-stiffness isolator", *J. Mech. Sci. Technol.*, **21**(6), 946. https://doi.org/10.1007/bf03027074

Carrella, A., Brennan, M.J. and Waters, T.P. (2007b), "Static analysis of a passive vibration isolator with quasi-zero-stiffness characteristic", *J. Sound Vib.*, **301**(3-5), 678-689. https://doi.org/10.1016/j.jsv.2006.10.011

Carrella, A., Brennan, M.J., Waters, T.P. and Shin, K. (2008), "On the design of a high-static–low-dynamic stiffness isolator using linear mechanical springs and magnets", *J. Sound Vib.*, **315**(3), 712-720. https://doi.org/10.1016/j.jsv.2008.01.046

Cheng, C., Li, S., Wang, Y. and Jiang, X. (2016), "On the analysis of a high-static-low-dynamic stiffness vibration isolator with time-delayed cubic displacement feedback", *J. Sound Vib.*, **378**(2016), 76-91. https://doi.org/10.1016/j.jsv.2016.05.029

Chronopoulos, D., Antoniadis, I. and Ampatzidis, T. (2017), "Enhanced acoustic insulation properties of composite metamaterials having embedded negative stiffness inclusions", *Extreme Mech. Lett.*, **12**, 48-54. https://doi.org/10.1016/j.eml.2016.10.012

Fulcher, B.A., Shahan, D.W., Haberman, M.R., Conner Seepersad, C. and Wilson, P.S. (2014), "Analytical and experimental investigation of buckled beams as negative stiffness elements for passive vibration and shock isolation systems", *J. Vib. Acoust.*, **136**(3). https://doi.org/10.1115/1.4026888

Huang, X., Liu, X., Sun, J., Zhang, Z. and Hua, H. (2014), "Vibration isolation characteristics of a nonlinear isolator using Euler buckled beam as negative stiffness corrector: A theoretical and experimental study", *J. Sound Vib.*, **333**(4), 1132-1148. https://doi.org/10.1016/j.jsv.2013.10.026

Iemura, H. and Pradono, M.H. (2009), "Advances in the development of pseudo-negative-stiffness dampers for seismic response control", *Struct. Control Health Monitor.*, **16**(7-8), 784-799. https://doi.org/10.1002/stc.345

Iemura, H., Kouchiyama, O., Toyooka, A. and Shimoda, I. (2008), "Development of the friction-based passive negative stiffness damper and its verification tests using shaking table", *Proceedings of the 14th World Conference on Earthquake Engineering*, Vol. 12, pp. 01-0219.

Kashdan, L., Conner Seepersad, C., Haberman, M. and Wilson, P.S. (2012), "Design, fabrication, and evaluation of negative stiffness elements using SLS", *Rapid Prototyping J.*, **18**(3), 194-200. https://doi.org/10.1108/13552541211218108

Kelly, J.M. (1999), "The role of damping in seismic isolation", *Earthq. Eng. Struct. Dyn.*, **28**(1), 3-20. https://doi.org/10.1002/(SICI)1096-9845(199901)28:1<3::AID-EQE801>3.0.CO;2-D

Lan, C.-C., Yang, S.-A. and Wu, Y.-S. (2014), "Design and experiment of a compact quasi-zero-stiffness isolator capable of a wide range of loads", *J. Sound Vib.*, **333**(20), 4843-4858. https://doi.org/10.1016/j.jsv.2014.05.009

Le, T.D. and Ahn, K.K. (2011), "A vibration isolation system in low frequency excitation region using negative stiffness structure for vehicle seat", *J. Sound Vib.*, **330**(26), 6311-6335. https://doi.org/10.1016/j.jsv.2011.07.039

Li, H.-N., Sun, T., Lai, Z. and Nagarajaiah, S. (2018), "Effectiveness of negative stiffness system in the benchmark structural-control problem for seismically excited highway bridges", *J. Bridge Eng.*, **23**(3), 04018001. https://doi.org/10.1061/(asce)be.1943-5592.0001136

Li, H., Li, Y. and Li, J. (2020), "Negative stiffness devices for

vibration isolation applications: A review", *Adv. Struct. Eng.*, **23**(8), 1739-1755. https://doi.org/10.1177/1369433219900311

Liu, X., Huang, X. and Hua, H. (2013), "On the characteristics of a quasi-zero stiffness isolator using Euler buckled beam as negative stiffness corrector", *J. Sound Vib.*, **332**(14), 3359-3376. https://doi.org/10.1016/j.jsv.2012.10.037

Lu, L.-Y. and Lin, G.-L. (2009), "Improvement of near-fault seismic isolation using a resettable variable stiffness damper", *Eng. Struct.*, **31**(9), 2097-2114. https://doi.org/10.1016/j.engstruct.2009.03.011

Malatkar, P. and Nayfeh, A. (2002), "Calculation of the jump frequencies in the response of sdof non-linear systems", *J. Sound Vib.*, **254**, 1005-1011. https://doi.org/10.1006/jsvi.2001.4104

Mizuno, T., Takasaki, M., Kishita, D. and Hirakawa, K. (2007), "Vibration isolation system combining zero-power magnetic suspension with springs", *Control Eng. Practice*, **15**(2), 187-196. https://doi.org/10.1016/j.conengprac.2006.06.001

Molyneux, W. (1958), "The support of an aircraft for ground resonance tests: a survey of available methods", *Aircr. Eng. Aerosp. Technol.*, **30**(6), 160-166. https://doi.org/10.1108/eb032976

Niu, F., Meng, L., Wu, W., Sun, J., Zhang, W., Meng, G. and Rao, Z. (2014), "Design and analysis of a quasi-zero stiffness isolator using a slotted conical disk spring as negative stiffness structure", *J. Vibroeng.*, **16**(4), 1769-1785.

Piersol, A.G. and Harris, C.M. (2017), *Harri's Shock and Vibration Handbook*, Fifth Edition, McGraw-Hill.

Ravindra, B. and Mallik, A. (1994), "Performance of non-linear vibration isolators under harmonic excitation", *J. Sound Vib.*, **170**(3), 325-337. https://doi.org/10.1006/jsvi.1994.1066

Shi, X. and Zhu, S. (2015), "Magnetic negative stiffness dampers", *Smart Mater. Struct.*, **24**(7), 072002. https://doi.org/10.1088/0964-1726/24/7/072002

Shi, X., Zhu, S., Ni, Y. and Li, J. (2018), "Vibration suppression in high-speed trains with negative stiffness dampers", *Smart Struct. Syst., Int. J.*, **21**(5), 653-668. https://doi.org/10.12989/sss.2018.21.5.653

Shi, X., Shi, W. and Xing, L. (2019), "Performance analysis of vehicle suspension systems with negative stiffness", *Smart Struct. Syst., Int. J.*, **24**(1), 141-155. https://doi.org/10.12989/sss.2019.24.1.141

Sun, T., Lai, Z., Nagarajaiah, S. and Li, H.N. (2017), "Negative stiffness device for seismic protection of smart base isolated benchmark building", *Struct. Control Health Monitor.*, **24**(11), e1968. https://doi.org/10.1002/stc.1968

Toyooka, A., Motoyama, H., Kouchiyama, O. and Iwasaki, Y. (2015), "Development of autonomous negative stiffness damper for reducing absolute responses", *Quarterly Report of RTRI*, **56**(4), 284-290. https://doi.org/10.2219/rtriqr.56.4_284

Viti, S., Cimellaro, G.P. and Reinhorn, A.M. (2006), "Retrofit of a hospital through strength reduction and enhanced damping", *Smart Struct. Syst., Int. J.*, **2**(4), 339-355. https://doi.org/10.12989/sss.2006.2.4.339

Winterflood, J., Blair, D.G. and Slagmolen, B. (2002), "High performance vibration isolation using springs in Euler column buckling mode", *Phys. Lett. A*, **300**(2-3), 122-130. https://doi.org/10.1016/s0375-9601(02)00258-x

Xiang, S. and Songye, Z. (2019), "A comparative study of vibration isolation performance using negative stiffness and inerter dampers", *J. Franklin Inst.*, **356**(14), 7922-7946. https://doi.org/10.1016/j.jfranklin.2019.02.040

Xu, D., Yu, Q., Zhou, J. and Bishop, S.R. (2013), "Theoretical and experimental analyses of a nonlinear magnetic vibration isolator with quasi-zero-stiffness characteristic", *J. Sound Vib.*, **332**(14), 3377-3389. https://doi.org/10.1016/j.jsv.2013.01.034

Yu, Y., Li, J., Li, Y., Li, S., Li, H. and Wang, W. (2019a), "Comparative investigation of phenomenological modeling for hysteresis responses of magnetorheological elastomer devices", *Int. J. Molecular Sci.*, **20**(13), 3216. https://doi.org/10.3390/ijms20133216

Yu, Y., Li, Y., Li, J. and Gu, X. (2019b), "Characterizing nonlinear oscillation behavior of an MRF variable rotational stiffness device", *Smart Struct. Syst., Int. J.*, **24**(3), 303-317. https://doi.org/10.12989/sss.2019.24.3.303

Yu, Y., Royel, S., Li, Y., Li, J., Yousefi, A.M., Gu, X., Li, S. and Li, H. (2020), "Dynamic modelling and control of shear-mode rotational MR damper for mitigating hazard vibration of building structures", *Smart Mater. Struct.*, **29**(11), 114006. https://doi.org/10.1088/1361-665X/abb573

Zheng, Y., Zhang, X., Luo, Y., Yan, B. and Ma, C. (2016), "Design and experiment of a high-static–low-dynamic stiffness isolator using a negative stiffness magnetic spring", *J. Sound Vib.*, **360**, 31-52. https://doi.org/10.1016/j.jsv.2015.09.019

Zheng, Y., Zhang, X., Luo, Y., Zhang, Y. and Xie, S. (2018), "Analytical study of a quasi-zero stiffness coupling using a torsion magnetic spring with negative stiffness", *Mech. Syst. Signal Process.*, **100**, 135-151. https://doi.org/10.1016/j.ymssp.2017.07.028

Zhou, J., Wang, X., Xu, D. and Bishop, S. (2015), "Nonlinear dynamic characteristics of a quasi-zero stiffness vibration isolator with cam–roller–spring mechanisms", *J. Sound Vib.*, **346**, 53-69. https://doi.org/10.1016/j.jsv.2015.02.005

HJ